





ORIGINAL RESEARCH

# Amyloid Deposits and Fibrosis on Left Ventricular Endomyocardial Biopsy Correlate With Extracellular Volume in Cardiac Amyloidosis

Angela Pucci, MD, PhD\*; Alberto Aimò, MD\*; Veronica Musetti, BSc; Andrea Barison , MD, PhD; Giuseppe Vergaro, MD, PhD; Dario Genovesi, MD; Assuero Giorgetti , MD; Silvia Masotti, PhD; Chiara Arzilli, MD; Concetta Prontera, BSc; Luigi Emilio Pastormerlo, MD, PhD; Michele Alessandro Coceani, MD; Marco Ciardetti , MD; Nicola Martini, PhD; Cataldo Palmieri, MD; Claudio Passino, MD; Claudio Rapezzi, MD; Michele Emdin , MD, PhD

**BACKGROUND:** The relative contribution of amyloid and fibrosis to extracellular volume expansion in cardiac amyloidosis (CA) has never been defined.

**METHODS AND RESULTS:** We included all patients diagnosed with amyloid light-chain (AL) or transthyretin cardiac amyloidosis at a tertiary referral center between 2014 to 2020 and undergoing a left ventricular endomyocardial biopsy. Patients (n=37) were more often men (92%), with a median age of 72 years (interquartile range, 68–81). Lambda-positive AL was found in 14 of 19 AL cases (38%) and kappa-positive AL in 5 of 19 (14%), while transthyretin was detected in the other 18 cases (48%). Amyloid deposits accounted for 15% of tissue sample area (10%–30%), without significant differences between AL and transthyretin amyloidosis. All patients displayed myocardial fibrosis, with a median extent of 15% of tissue samples (10%–23%; range, 5%–60%), in the absence of spatial overlap with amyloid deposits. Interstitial fibrosis was often associated with mild and focal subendocardial fibrosis. The extent of fibrosis or the combination of amyloidosis and fibrosis did not differ significantly between transthyretin amyloidosis and AL subgroups. In 20 patients with myocardial T1 mapping at cardiac magnetic resonance, the combined amyloid and fibrosis extent displayed a modest correlation with extracellular volume ( $r=0.661$ ,  $P=0.001$ ). The combined amyloid and fibrosis extent correlated with high-sensitivity troponin T ( $P=0.035$ ) and N-terminal pro-B-type natriuretic peptide ( $P=0.002$ ) serum levels.

**CONCLUSIONS:** Extracellular spaces in cardiac amyloidosis are enlarged to a similar extent by amyloid deposits and fibrotic tissue. Their combination can better explain the increased extracellular volume at cardiac magnetic resonance and circulating biomarkers than amyloid extent alone.

**Key Words:** amyloid ■ biomarkers ■ cardiac amyloidosis ■ cardiac magnetic resonance ■ endomyocardial biopsy ■ extracellular volume ■ fibrosis

**A**myloidosis is characterized by the extracellular deposition of amyloidogenic proteins in a beta-sheet structure with a typical green birefringence by Congo Red staining on polarized light microscopy.<sup>1</sup> Amyloid deposition may cause tissue

disruption and dysfunction, organ failure, and death.<sup>1</sup> Immunoglobulin light-chain and transthyretin amyloidosis (AL and ATTR, respectively) are those associated with the most clinically relevant forms of amyloid cardiac disease.<sup>1</sup>

Correspondence to: Michele Emdin, MD, PhD, FESC, Scuola Superiore Sant'Anna and Fondazione Toscana Gabriele Monasterio, Pisa, Italy. E-mails: emdin@ftgm.it, m.emdin@sssup.it

\*A. Pucci and A. Aimò contributed equally.

For Sources of Funding and Disclosures, see page 10.

© 2021 The Authors. Published on behalf of the American Heart Association, Inc., by Wiley. This is an open access article under the terms of the Creative Commons Attribution-NonCommercial-NoDerivs License, which permits use and distribution in any medium, provided the original work is properly cited, the use is non-commercial and no modifications or adaptations are made.

JAHA is available at: [www.ahajournals.org/journal/jaha](http://www.ahajournals.org/journal/jaha)

## CLINICAL PERSPECTIVE

### What Is New?

- Patients with cardiac amyloidosis have an increased extracellular volume.
- This is attributable to amyloid deposits and fibrotic tissue.

### What Are the Clinical Implications?

- The combination of amyloid and fibrosis can better explain the increased extracellular volume at cardiac magnetic resonance and circulating biomarkers than amyloid extent alone.

## Nonstandard Abbreviations and Acronyms

<b>AL</b>	light-chain amyloidosis
<b>ATTR</b>	transthyretin amyloidosis
<b>CA</b>	cardiac amyloidosis
<b>ECV</b>	extracellular volume
<b>EMB</b>	endomyocardial biopsy
<b>hs-TnT</b>	high-sensitivity troponin T
<b>LGE</b>	late gadolinium enhancement
<b>sST2</b>	soluble suppression of tumorigenesis-2

Accurate diagnosis of cardiac amyloidosis (CA) and characterization of the amyloid precursor are crucial for treatment. Endomyocardial biopsy (EMB) remains the gold standard to assess the pathophysiological details of CA in vivo, as well as to provide unique insights into what is observed with noninvasive in vivo imaging techniques, such as cardiac magnetic resonance (CMR) and nuclear medicine.<sup>2-5</sup> Currently, EMB is performed only in experienced centers and usually in the right ventricle.<sup>6,7</sup> Nevertheless, left ventricular (LV) EMB presents a low risk of complications, particularly when performed with a transradial approach<sup>6</sup>; moreover, LV EMB might also be more sensitive in the detection of earlier subendocardial histopathological changes compared with right ventricular EMB.<sup>7</sup>

In the present study, we investigated the correlates of LV EMB findings in patients with AL or ATTR CA. In particular, the presence and extent of amyloid deposits, fibrosis, and inflammatory infiltrates were compared with CMR evaluation of extracellular volume (ECV) and other imaging and laboratory findings.

## METHODS

### Study Population

All patients with EMB-proven diagnosis of AL or ATTR between 2014 to 2020 were identified in the electronic records of a tertiary referral center (Fondazione Toscana Gabriele Monasterio, Pisa, Italy). Among these patients (n=37), 29 (78%) had undergone CMR and 35 (95%) myocardial diphosphonate scintigraphy. NT-proBNP (N-terminal pro-B-type natriuretic peptide) and high-sensitivity troponin T (hs-TnT) were measured in all patients before the EMB, and soluble suppression of tumorigenesis-2 (sST2) in 24 (65%). The study complied with the Declaration of Helsinki and was approved by the Institutional Review Board. The data that support the findings of this study are available from the corresponding author upon reasonable request.

### Endomyocardial Biopsy Work-Up

#### Sampling of the Myocardium

All EMBs were performed to assess the diagnosis of CA. The Cordis bioptome forceps was introduced in the left ventricle through the femoral artery and used to take at least 3 endomyocardial samples in different areas of the left ventricle. Contrast medium was injected at the end of the procedure to exclude iatrogenic mitral regurgitation and pericardial effusion.<sup>7</sup> All EMBs were performed within 1 week of the CMR, and sampling was blinded to CMR results.

### Histology, Immunohistochemistry, and Morphometry Analyses

All EMBs were adequately fixed and without artifacts. EMB samples were formalin fixed for 1 to 2 hours, then paraffin embedded. Serial sections were obtained from a single block inclusion.<sup>8</sup> Congo red, Masson's trichrome, and Perls' histochemical stains were performed, together with immunohistochemistry by using immunoperoxidase technique and specific antibodies against leukocyte antigens (CD3, CD20, KP1; Dakopatts Ltd.), kappa and lambda light chains (Ventana) and transthyretin (Dako). Slides were deparaffinized and brought to water, then primary specific antibodies were applied, and single immunostainings were revealed by using the biotin-free, multimer molecule-based Ultraview Universal DAB Detection Kit for the detection of mouse and rabbit primary antibodies (Roche). Congo red staining was analyzed by a polarized light microscope (Ris-D2Nikon) that detected amyloid as green birefringent deposits, whereas fibrosis was evidenced as intense blue-stained (interstitial or subendocardial) areas on Masson's trichrome staining. All EMBs were serially sectioned.<sup>8</sup> Amyloid deposits were analyzed on a Congo red-stained slide, and

fibrous tissue on an adjacent Masson's trichrome-stained slide.

Amyloid deposits, fibrosis, inflammatory cells (T-lymphocytes: CD3+; monocyte-macrophages: CD68+), light chains, and transthyretin immunoreactive deposits were quantitatively evaluated by morphometric analysis, using the NIS-Elements computer-assisted image analysis system (Nikon). Total area of biopsy fragments was calculated for each EMB; total amyloid (Congo red-positive) deposits, and total interstitial fibrosis (on Masson's trichrome) areas were expressed as percentages. Inflammatory infiltrates were quantified as number of cells/mm<sup>2</sup>.

### Histology Score

A semiquantitative histology score was assigned to each EMB, to take into account the amyloid deposition, the fibrosis extent, and the inflammatory infiltration, as follows: for either (1) amyloid deposition or (2) fibrosis extent: 0 (absent), 1 (1%–5% of total EMB area), 2 (6%–15%), 3 (16%–30%) and 4 (>30%); for either (3) T lymphocytes (CD3+ cells), or (4) for monocytes/macrophages: 0 (absent), 1 (1–6 cells/mm<sup>2</sup>), 2 (7–15/mm<sup>2</sup>), 3 (>15/mm<sup>2</sup>).

### Transthoracic Echocardiography

Two-dimensional transthoracic echocardiography images were obtained using a Philips IE33 ultrasound machine, with X5-1 transducer (Philips Medical Systems, Palo Alto, CA) and interpreted according to the American Society of Echocardiography/European Association of Cardiovascular Imaging guidelines.<sup>9</sup>

### Cardiac Magnetic Resonance

Patients underwent CMR with a 32-channel phased-array surface receiver coil and vectorcardiogram triggering using a 1.5 T scanner (Signa Excite, GE Healthcare, Milwaukee, WI). Biventricular systolic function was assessed by breath-hold steady-state free precession cine imaging in the short-axis stack (8-mm thickness, no gap). Sequence parameters were field of view, 360 to 400 mm; repetition/echo time, 3.2/1.6 ms; flip angle, 45 to 60°, matrix, 224×224; phases, 30. In 28 of 29 patients, Late gadolinium enhancement (LGE) imaging was performed between 10 and 20 minutes after contrast agent administration (gadoteric acid, DOTAREM, 0.2 mmol/kg) using a segmented T1-weighted gradient-echo inversion-recovery pulse sequence. In short-axis orientation, the left ventricle was encompassed by contiguous 8-mm thick slices (with no interslice gap). Inversion time was individually adapted to suppress the signal of normal remote myocardium (220–320 ms). Sequence parameters were field of view, 360 to 400 mm; slice thickness, 8 mm;

repetition/echo time, 4.6/1.3 ms; flip angle, 15 to 20°; matrix, 224×192. A midventricular short-axis inversion time-scout sequence was used to choose the appropriate inversion time. T1 mapping was acquired in basal, medium, and apical slices using a modified Look-Locker (MOLLI) sequence (3,3,5 scheme; flip angle, 35°; matrix, 172×172 pixels; partial Fourier=0.75) in 20 of 29 patients undergoing CMR; T1 mapping was acquired both precontrast (native) and postcontrast (15–20 minutes after gadolinium injection).

All CMR studies were analyzed offline on the Advantage Workstation (GE Healthcare) with a dedicated software (MASS 6.1, Medis, Leiden, Netherlands) by an experienced CMR reader (A.B.) blinded to all other patient data. LV and right ventricular volumes, mass, and global function were calculated on short-axis cine images.<sup>10</sup> LGE presence and patterns were visually assessed. Five LV regions were considered: anterior (segments 1 and 7), septal (segments 2, 3, 8, and 9), inferior (segments 4 and 10), lateral (segments 5, 6, 11, and 12) and apical (segments 13–17). The LGE pattern was classified as 0 (absent), 1 (patchy), 2 (subendocardial), or 3 (transmural). A global LGE score was obtained by summing the 5 regional scores. Blood-pool early darkening was defined as a signal intensity decay >50% during the first 10 minutes after gadolinium injection at LGE images acquired with a fixed inversion time.<sup>11</sup> In 20 patients, native and postcontrast T1 mapping was analyzed by drawing a region of interest in the septum (segments 2, 3, 8, 9, and 14). ECV was calculated from  $(\Delta R1_{\text{myocardium}}/\Delta R1_{\text{blood}}) \times (1 - \text{hematocrit})$ , where  $\Delta R1 = (1/T1_{\text{postcontrast}} - 1/T1_{\text{precontrast}})$ .<sup>12</sup> Total LV matrix and cell volumes were calculated from the product of LV myocardial volume (LV mass divided by the specific gravity of myocardium [1.05 g/mL]) and ECV or (1–ECV), respectively.<sup>13</sup>

### Laboratory Evaluation

NT-proBNP and hs-TnT were measured on plasma EDTA and lithium heparin samples, respectively, using electrochemiluminescence immunoassays on automated Cobas analyzers (Elecsys proBNP II and Elecsys Troponin Gen5STAT, Roche Diagnostics, Germany).<sup>14,15</sup> Soluble suppression of tumorigenesis 2 (sST2) was measured on plasma EDTA samples using the Presage assay (Critical Diagnostics, San Diego, CA).<sup>16,17</sup>

### Statistical Analysis

Statistical analysis was performed using IBM SPSS Statistics (version 22, 2013). Normal distribution was assessed through the Kolmogorov-Smirnov test; all variables had nonnormal distribution and were then expressed as median and interquartile interval.

Differences between groups were tested through the Mann-Whitney *U* test, and categorical variables were compared by the chi-square test with Yates correction. To assess the strength of correlations, variables were ln-transformed, and Pearson's *r* values were calculated. Linear regression analysis was also performed using ln-transformed variables. *P*<0.05 was considered statistically significant.

## RESULTS

### Patient Population

The main clinical, laboratory, and CMR findings are reported in Table 1. The majority of patients (92%) were men, with a median age of 72 years (interquartile range, 68–81). Both NT-proBNP and hs-TnT were markedly elevated (6772 ng/L [2071–12 557] and 62 ng/L [38–140],

**Table 1. Findings From Clinical, Laboratory, and Imaging Examinations**

	All patients n=37	AL n=19 (51%)	ATTR n=18 (49%)	P Value
Men, n (%)	34 (92)	17 (90)	17 (94)	0.580
Age, years, interquartile range	72 (68–81)	69 (67–74)	76 (70–83)	0.024
eGFR, mL/min per 1.73 m <sup>2</sup>	67 (45–79)	61 (42–79)	71 (55–79)	0.199
NYHA class I–III/III–IV, n (%)	15/22 (41/59)	7/12 (37/63)	8/10 (44/56)	0.638
Hematocrit (%)	36 (34–40)	36 (34–40)	36 (35–40)	0.897
NT-proBNP, ng/L	6772 (2071–12 557)	10 164 (1912–16 874)	3750 (2361–8592)	0.118
hs-TnT, ng/L	62 (38–140)	95 (37–207)	54 (38–93)	0.134
sST2, ng/mL	27 (16–37)	21 (14–32)	32 (21–45)	0.167
TTE				
E/e'	17 (12–24)	15 (12–25)	18 (12–23)	0.916
LAVi, mL/m <sup>2</sup>	24 (21–28)	24 (21–28)	25 (20–29)	0.618
Moderate/severe aortic stenosis	2 (5)	1 (5)	1 (6)	0.969
TAPSE	17 (13–22)	17 (14–24)	16 (13–22)	0.586
CMR				
LVEDVi, mL/m <sup>2</sup>	79 (68–92)	78 (62–90)	80 (73–94)	0.374
LVESVi, mL/m <sup>2</sup>	32 (28–43)	32 (23–45)	32 (30–40)	0.531
SVi, mL/m <sup>2</sup>	42 (32–51)	38 (28–49)	46 (36–55)	0.232
LVEF (%)	54 (45–62)	52 (45–56)	58 (42–63)	0.449
LVMI, g/m <sup>2</sup>	112 (102–143)	109 (91–115)	140 (110–153)	0.022
IVS, mm	19 (17–21)	18 (15–21)	20 (17–22)	0.199
PW, mm	15 (12–16)	15 (12–19)	15 (12–16)	0.880
RVEDVi, mL/m <sup>2</sup>	76 (65–92)	77 (65–89)	71 (65–98)	0.746
RVEF, %	55 (44–64)	51 (43–63)	55 (45–67)	0.589
Small LGE areas, n (%)	4/28 (14)	3/15 (20)	1/13 (8)	0.594
Subendocardial LGE, n (%)	9/28 (32)	5/15 (33)	4/13 (31)	
Transmural LGE, n (%)	15/28 (54)	7/15 (47)	8/13 (61)	
LGE score	10 (7–13)	10 (6–14)	10 (8–13)	1.000
Blood-pool early darkening, n (%)	10/28 (36)	8/15 (53)	2/13 (15)	0.055
Native myocardial T1, ms <sup>†</sup>	1118 (1016–1196)	1191 (1118–1229)	1015 (972–1070)	0.036
ECV (%) <sup>†</sup>	54 (44–61)	54 (45–59)	54 (42–69)	0.972
Pericardial effusion, n (%)	9/29 (31)	7/16 (44)	2/13 (15)	0.130
Pleural effusion, n (%)	9/29 (31)	5/16 (31)	4/13 (31)	1.000

The interquartile interval was reported in parentheses.

AL indicates amyloid light-chain amyloidosis; ATTR, amyloid transthyretin amyloidosis; CMR, cardiac magnetic resonance; ECV, extracellular volume; eGFR, estimated glomerular filtration rate; hs-TnT, high-sensitivity troponin T; IVS, interventricular septum; LAVi, left atrial volume index; LGE, late gadolinium enhancement; LVEDVi, left ventricular end-diastolic volume index; LVEF, left ventricular ejection fraction; LVESVi, left ventricular end-systolic volume index; LVMI, left ventricular mass index; NT-proBNP, N-terminal pro-B-type natriuretic peptide; NYHA, New York Heart Association; PW, posterior wall thickness; RVEDVi, right ventricular end-diastolic volume index; RVEF, right ventricular ejection fraction; sST2, soluble suppression of tumorigenesis-2; SVi, stroke volume index; TAPSE, tricuspid annular plane systolic excursion; and TTE, transthoracic echocardiography.

<sup>†</sup>Myocardial T1, ECV, matrix volume, and cell volume were available only in 20 subjects.

respectively), while median sST2 (27 ng/mL [16–37]) was below the threshold for risk prediction in chronic heart failure (35 ng/mL).<sup>17</sup> Echocardiographic E/e' ratio was 17, suggesting an initial impairment of diastolic function.

No significant differences in clinical, laboratory, scintigraphy, and histology findings were observed in patients undergoing or not undergoing CMR (Table S1). At CMR examination, all patients displayed septal hypertrophy ( $\geq 13$  mm), and 23 (79%) had an increased LV mass index; systolic function was reduced (LV ejection fraction  $< 50\%$ ) in 11 patients (38%) and borderline (ejection fraction 50%–55%) in 5 (17%). All patients had LGE areas, typically with subendocardial ( $n=9$ ; 32%) or transmural distribution ( $n=15$ ; 54%), with a median LGE score of 10 of 15. Median ECV was 54%, in patients with AL as well as in ATTR, well above the upper reference value from the literature (29%)<sup>4,5</sup> (Figure S1).

Only 2 patients had ATTRv (mutations: p.Val142Ile and p.Ile88Leu). Patients diagnosed with AL amyloidosis ( $n=19$ ; 51%) were younger, had lower LV mass values, and displayed more often early darkening than those with ATTR amyloidosis, while LGE patterns and ECV values were similar. As expected, they less often displayed cardiac diphosphonate uptake (Table 1).

## Endomyocardial Biopsy Findings

EMB findings of individual patients are reported in Table S2. Three tissue samples were available for each patient, except for 2 patients having 4 samples. At immunohistochemistry, lambda-positive AL was found in 14 of 19 (38%) and kappa-positive AL in 5 of 19 patients (14%) (Figure S2). Transthyretin immunoreactivity was detected in the remaining 18 patients (48%). Three patients classified as having

ATTR displayed a weak positivity for AL, deemed nonspecific; 3 other patients diagnosed with AL had a nonspecific positivity for ATTR. Nodular amyloid deposits were uncommon, detected in only one AL (kappa-positive) EMB.

In the whole cohort, amyloid deposits accounted for 15% of the tissue sample area (interquartile range, 10%–30%; range, 5%–60%; averaged coefficient of variation, 29.7%), with no significant difference between the AL and ATTR subgroups (Table 2). Amyloid deposition was multifocal in 78% of patients and diffuse in 11%, and amyloid fibers were found in both interstitial and perivascular spaces in 62%, with no significant differences between AL and ATTR. Nonetheless, transthyretin-positive biopsies showed a tendency to a patchy, coarse distribution of amyloid deposits, which was observed in 11 of 18 transthyretin-positive EMBs and in 7 of 19 of AL EMBs. Areas of AL kappa or lambda and transthyretin immunoreactivity were larger than areas of Congo red green birefringence (Figure 1).

All patients displayed myocardial fibrosis, with a median extent of 15% of tissue samples (interquartile range, 10%–23%, range, 5%–60%, averaged coefficient of variation, 24.6%), and no spatial overlap with amyloid deposition (Figure 2). On Masson's trichrome staining, amyloid could be identified by a blue-gray color as compared with the strong blue color of either interstitial or endocardial fibrosis, as previously shown in lung amyloidosis.<sup>18</sup> Fibrosis showed an interstitial pattern and was often associated with mild and focal subendocardial fibrosis (Figure S3). The extent of fibrosis or the combination of amyloidosis and fibrosis did not show any statistically significant difference between the ATTR and AL subgroups.

**Table 2. Histologic Findings**

	All patients n=37	AL n=19 (51%)	ATTR n=18 (49%)	P Value
Extent of amyloid deposits (%)	15 (10–30)	20 (10–30)	15 (9–43)	0.869
Amyloid pattern, n (%)				
Minimal	3 (8)	1 (5)	2 (11)	0.719
Focal	1 (3)	1 (5)	0 (0)	
Multifocal	29 (78)	15 (79)	14 (78)	
Diffuse	4 (11)	2 (11)	2 (11)	
Amyloid location, n (%)				
Interstitial	11 (30)	6 (32)	5 (28)	0.177
Interstitial and perivascular	23 (62)	10 (53)	13 (72)	
Interstitial, perivascular, vascular	3 (8)	3 (16)	0 (0)	
Histology score	9 (8–10)	9 (8–11)	8 (7–9)	0.030
Extent of fibrosis (%)	15 (10–23)	10 (10–20)	19 (12–26)	0.163
Extent of amyloidosis and fibrosis (%)	40 (30–49)	40 (21–45)	42 (32–51)	0.313
CD3+, cells/mm <sup>3</sup>	6 (5–10)	8 (5–10)	5 (2–6)	0.035
CD68+, cells/mm <sup>3</sup>	11 (7–16)	12 (7–18)	10 (5–18)	0.147

AL indicates amyloid light chain amyloidosis; and ATTR, amyloid transthyretin amyloidosis.

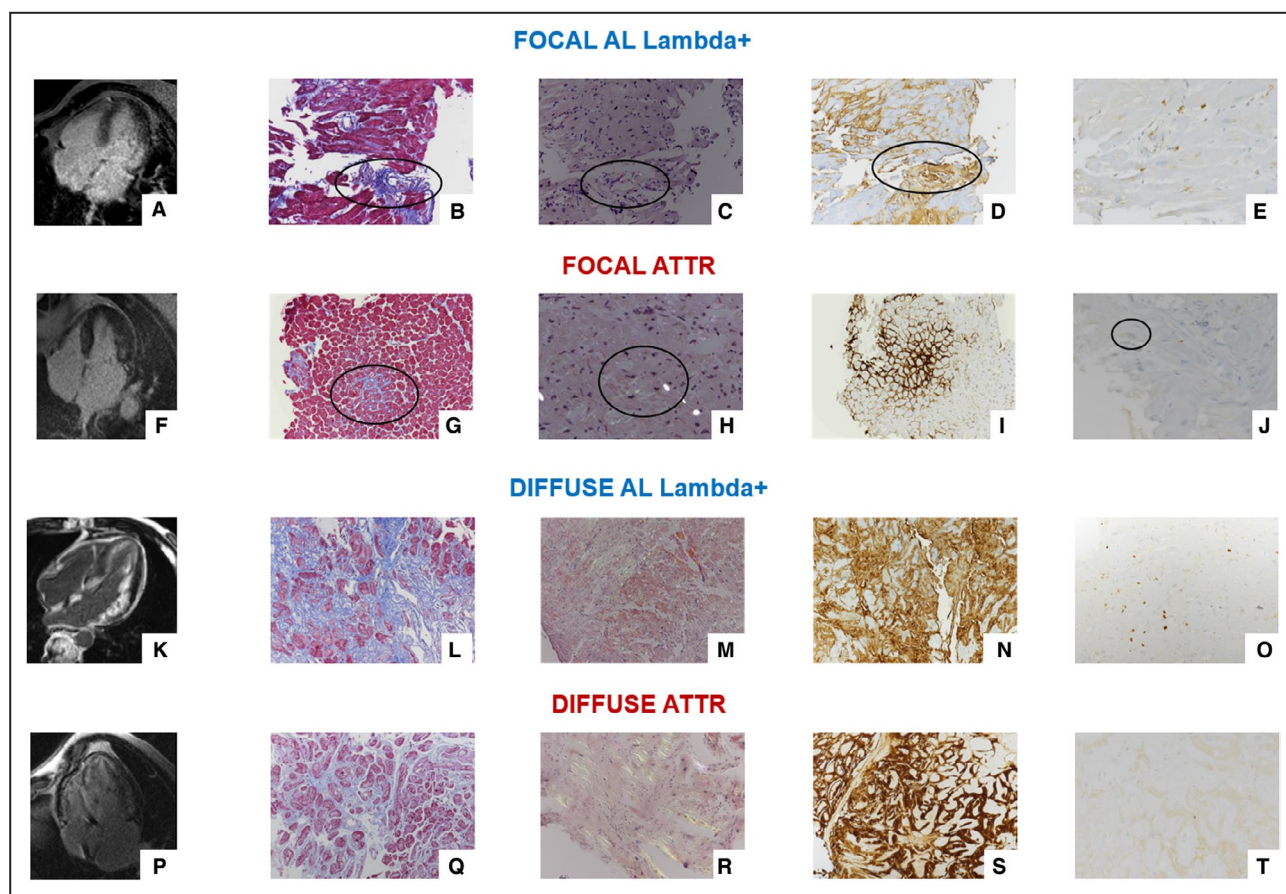


**Figure 1. Late gadolinium enhancement, histologic, and immunohistochemical findings in patients with focal and diffuse amyloid deposition.**

Cardiac magnetic resonance 4-chamber views (A, F, K, and P) and left ventricular endomyocardial biopsy fragments showing focal interstitial (B and G) or diffuse fibrosis (L and Q) by Masson's trichrome staining, and focal (C and H) or diffuse (M and R) green refringent deposits by Congo red staining under polarized light, focal (D and I) or diffuse (N and S) immunoreactivity for lambda light-chain (AL) or transthyretin (ATTR) deposits, and a few (E and J) or multifocal (O and T) CD3+ T-lymphocytes (B, G, L, and Q: Masson's trichrome staining, original magnification: B and G  $\times 10$ , I and O  $\times 20$ ; C, H, M, and R: Congo red staining under polarized light, original magnification: C  $\times 10$ , H, M, and R  $\times 20$ ; D and N: immunoperoxidase staining with hematoxylin counterstaining for lambda light-chain, original magnification: D  $\times 10$ , N  $\times 20$ ; I and S, immunoperoxidase staining with hematoxylin counterstaining for transthyretin, original magnification I  $\times 10$ , S  $\times 20$ ; E, J, O, and T, immunoperoxidase staining with hematoxylin counterstaining for CD3+ T-lymphocyte antigen, original magnification  $\times 20$ ).

Median histology score of overall EMBs was 9 of 14; patients with AL had a higher histology score as compared with patients with ATTR ( $P=0.03$ ). CD3+ cell density (cells/mm<sup>2</sup>) was higher in AL than ATTR EMBs ( $P=0.035$ ), whereas values of CD68+ monocyte-macrophages were not significantly different (Table 2). Plurifocal interstitial CD3+ lymphocytes were more frequently found in AL lambda-positive CA, whereas very few scattered or single CD3+ lymphocytes were usually observed in transthyretin-positive CA (Figure S4).

### CMR Correlates of Histological Findings

Amyloid extent correlated with LGE scores and ECV values, both in the whole population and in the AL subgroup (Figures S5 and S6). The sum of amyloid and fibrosis displayed an even closer correlation with ECV,

particularly in patients with ATTR (Figure 3), while fibrosis alone did not ( $P=0.344$  in the whole population). LGE scores and ECV values differed across patterns of amyloid depositions ( $P=0.049$  and  $0.047$ , respectively), with higher values in patients with a multifocal or diffuse pattern; no differences were observed according to the preferential site of amyloid accumulation (data not shown). The sum of amyloid and fibrosis also displayed a correlation with LV matrix volume ( $r=0.548$ ,  $P=0.012$ ), but not with LV cell volume ( $r=0.089$ ,  $P=0.710$ ).

### Histology and Biomarkers

Amyloid extent correlated with hs-TnT, both in the whole population ( $r=0.542$ ,  $P=0.001$ ) and in the AL ( $P=0.006$ ,  $r=0.622$ ) and ATTR subgroups ( $P=0.014$ ,  $r=0.533$ ). It also predicted hs-TnT after adjustment for LV mass

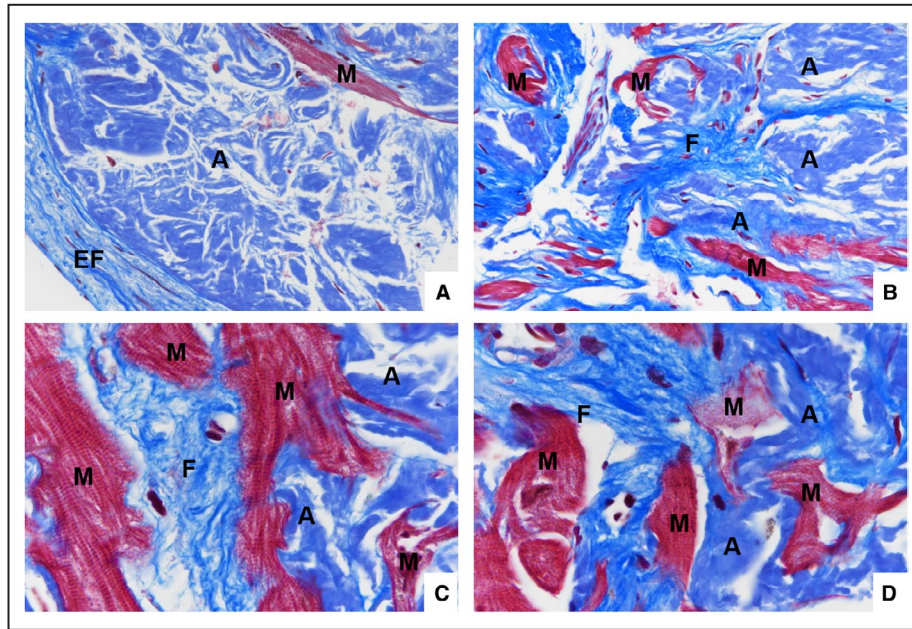


**Figure 2. Distribution of amyloid deposits and fibrosis.**

Endocardial (EF) and interstitial (F) fibrosis in the left ventricle endomyocardial biopsy from a transthyretin-positive (A and C) and a lambda+ AL (B and D) CA showing a brilliant, strong blue color by Masson's trichrome staining; it is associated with subendocardial and interstitial amyloid (A) deposits that stain blue-gray on the same Masson's trichrome staining. Myocytes (M) are encircled by fibrosis and by amyloid (Masson's trichrome staining; original magnification: A and B,  $\times 40$ , C and D,  $\times 100$ ).

index and LV ejection fraction, as confirmed in patients with AL (Table S3). Amyloid extent also independently predicted NT-proBNP, but not sST2, although the amyloid pattern or location did not predict circulating biomarkers. The combined amyloid and fibrosis extent also correlated with hs-TnT ( $P=0.035$ ) and NT-proBNP ( $P=0.002$ ), while the extent of fibrosis, histology score values, or CD3+ or CD68+ cell counts did not (Figure 4 and Table S3).

## DISCUSSION

To the best of our knowledge, this is the first series of patients undergoing only LV EMB for the diagnosis of CA to establish a correlation between pathological processes involving the extracellular volume on biopsy specimens, ECV at CMR, and biomarkers reflecting cardiac damage. We report that, in patients with CA, the extracellular space occupied not only by amyloid substance, but also, and to a significant extent, by fibrotic tissue. The combination of amyloid and fibrosis displays a better correlation with ECV quantification by CMR than the extent of amyloid deposits alone. Finally, the combined extent of amyloid and fibrosis displays a good correlation with hs-TnT and NT-proBNP.

Cardiac fibroblasts internalize aggregated transthyretin *in vitro*,<sup>19</sup> and matrix metalloproteinases are

overexpressed in CA.<sup>20</sup> Both mechanisms may contribute to the expansion of extracellular spaces and to the development of interstitial, reactive fibrosis in response to tissue damage. Another possible mechanism of interstitial fibrosis in CA is coronary microvascular dysfunction, extensively documented in CMR studies,<sup>21</sup> which may be related to amyloid deposition in the perivascular and vascular spaces, to expanded extracellular spaces, and to capillary rarefaction. Microvascular dysfunction/rarefaction could cause subclinical ischemic damage, triggering fibrosis and extracellular matrix deposition. The greater metabolic demands of the left ventricle might explain why the few studies evaluating right ventricular biopsies never reported a large amount of fibrosis.<sup>22-24</sup> Cardiac amyloid load can be measured through immunohistochemical staining for light chains or transthyretin, or through Congo red staining, which is known to correspond to beta-sheet-oriented amyloid fibrils in both forms of CA. In this study, we preferred to measure amyloid extent following Congo red staining, also because we found a larger area of light chain or transthyretin immunostaining than Congo red staining (data not shown).

Nonischemic cardiac disorders do not homogeneously affect the myocardium,<sup>25</sup> as shown, for example, by the high coefficient of variation of fibrosis in idiopathic dilated cardiomyopathy (43%).<sup>26</sup> As expected, we found variability in the presence and distribution of

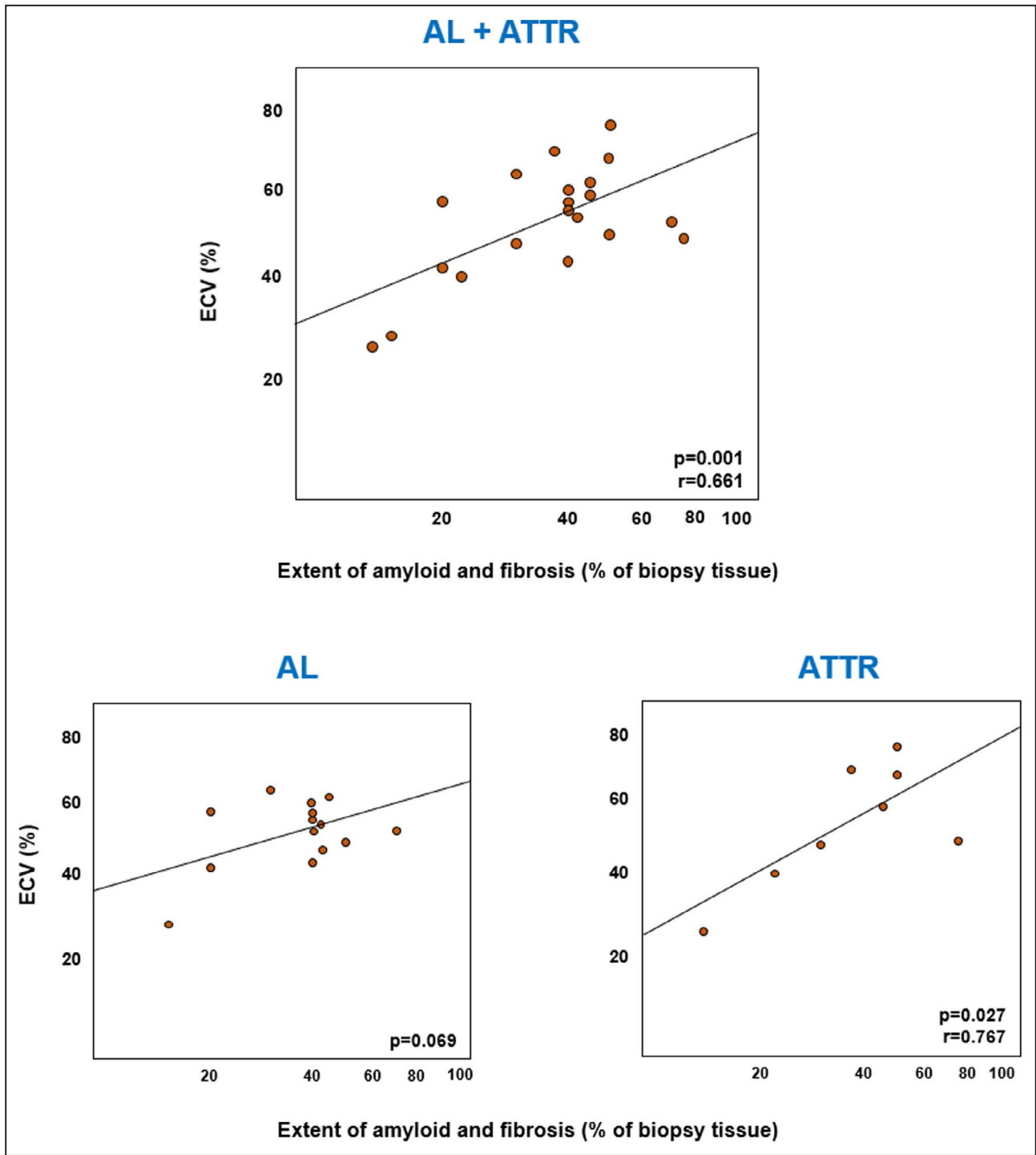


**Figure 3.** Correlations between the extent of amyloid and fibrotic deposits and extracellular volume (ECV). ECV values are in a log-scale. AL indicates amyloid light chain amyloidosis; and ATTR, amyloid transthyretin amyloidosis.

both amyloid deposits and collagen distribution. In particular, a few cases showed a high coefficient of variation related to their focal or segmental distribution. Spatial variation in small endomyocardial biopsies is expected to be high compared with ECV measurements that typically use larger volumes of myocardium. Additionally, the subendocardium is not included when calculating ECV,

while it is sampled by EMB. These limitations would reduce the ability to correlate CMR and EMB findings. Nonetheless, the extent of amyloid deposits or the combination of amyloid and fibrosis displayed rather close correlations with ECV.

This study provides a further histological validation of ECV measurement in CA, already demonstrated



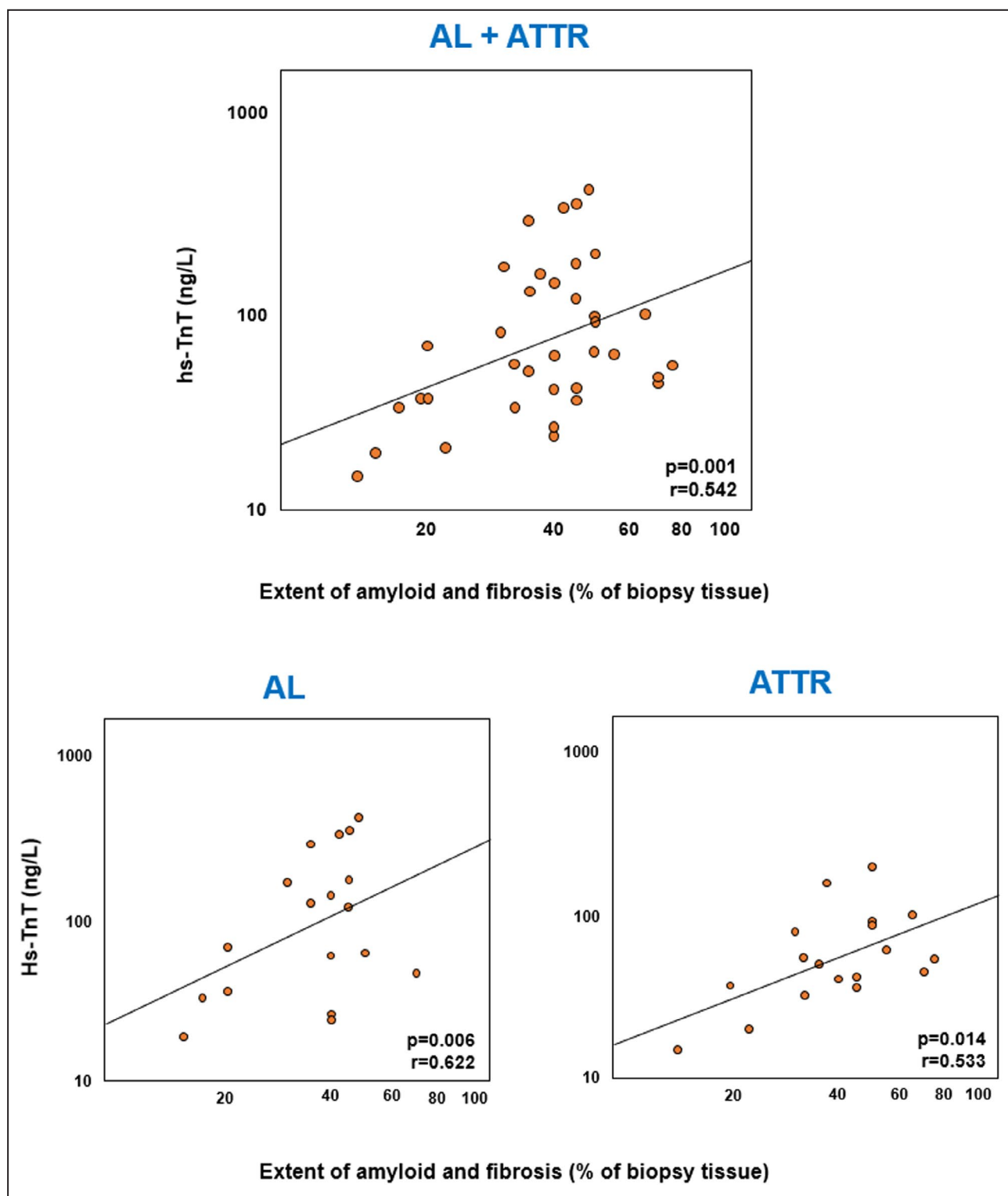


**Figure 4.** Correlations between the extent of amyloid and fibrosis and high-sensitivity troponin T (hs-TnT). hs-TnT values are in a log-scale. AL indicates amyloid light chain amyloidosis; and ATTR, amyloid transthyretin amyloidosis.

previously in a study on 9 patients with ATTR and 17 patients with AL.<sup>27</sup> Myocardial ECV provides an absolute quantification of interstitial expansion, beyond the semiquantitative assessment by conventional LGE.<sup>28-30</sup>

ECV is currently considered a marker of amyloid burden<sup>28-30</sup> and holds prognostic significance in both AL<sup>31</sup> and ATTR.<sup>28</sup> The amount of extracellular space in the interventricular septum estimated from pre- and

postcontrast T1 mapping showed a close relationship with the degree of extracellular matrix remodeling at histology, which was better represented by the sum of fibrosis and amyloidosis. LGE and ECV demonstrate an interstitial retention of gadolinium, which may be attributable to both fibrosis and amyloidosis. Notably, other possible causes of ECV expansion might be represented by extracellular edema, leukocyte activation, and microvascular abnormalities. This might explain why ECV tended to overestimate the sum of fibrosis and amyloidosis at histology. In a previous case series, the amount and transmural variation of amyloid protein at autopsy (subendocardial, 42%; subepicardial, 18%) was closely correlated with LGE at CMR, rather than to minor diffuse fibrosis (1.3%).<sup>32</sup> Conversely, in another study on 5 patients with CA undergoing CMR before heart transplantation, subendocardial and midwall LGE was significantly associated with fibrosis at histology, but not with amyloid deposits.<sup>33</sup> In our cohort, we confirmed that LGE is attributable to both interstitial amyloid deposition and fibrosis. The degree of extracellular volume expansion by amyloid substance and fibrosis independently predicted circulating hs-TnT and NT-proBNP, which are released following cardiomyocyte damage elicited by a mechanical or toxic effect of amyloid fibrils, and also by increased myocardial strain caused by pressure/volume overload. hs-TnT and NT-proBNP possess strong prognostic impact in patients with CA, particularly in AL.<sup>34</sup> Conversely, sST2, a biomarker that reflects the activation of inflammatory and profibrotic pathways, did not display a significant correlation with the severity of accumulation of amyloid and/or collagen fibers, possibly reflecting the fact that this biomarker is produced mainly outside of the heart.<sup>17</sup>

We report that amyloid deposits can show different patterns: diffuse or nodular, perivascular (at least in the initial stages) and interstitial (surrounding single myocytes). In both AL and transthyretin CA, Congo red positivity always had a more limited extent than immunohistochemical detection of light chains or transthyretin. To the best of our knowledge, this finding has never been described to date. We might hypothesize that deposition of amyloidogenic precursors, not organized in beta sheets, is far more diffuse in the myocardium than beta sheets of amyloid deposits.

Another novel aspect of the present study is represented by the histology score based on the EMB morphometric evaluation of amyloid deposits, fibrosis, and inflammatory infiltrates. Patients with AL had a higher histology score than patients with ATTR, which was associated with a higher CD3+ T-cell density. The presence of T histology lymphocytes denotes a subclinical inflammation contributing to the myocardial dysfunction in AL, likely related to direct toxic damage caused by light-chain deposits. These features suggest a more

severe impairment of myocardium in AL, corresponding to a more clinically severe disease as compared with ATTR. CD3+ T lymphocytes have been previously identified in AL and have been shown to predict adverse outcome in such patients.<sup>35</sup> In agreement with Siegismund et al, we did not find significant correlations between CD68+ macrophage counts and AL amyloidosis.

Immunohistochemistry for amyloid typing is often performed by postembedding immunogold electron microscopy that is considered a quite sensitive technique.<sup>2</sup> In our study, we used immunohistochemistry on formalin-fixed and paraffin-embedded EMBs obtaining clear-cut immunohistochemical results. Other series have shown that immunohistochemistry might overestimate the transthyretin immunoreactivity or misdiagnose the presence of immunoglobulin light chains.<sup>36</sup> We applied a restrictive fixation protocol (ie, all EMBs were formalin fixed for 1 to 2 hours only avoiding overfixation artifacts) and we considered kappa or lambda immunostaining as positive only when the other one was negative (so-called monotypic restriction used in hematopathology).<sup>37</sup>

Several limitations must be acknowledged. First, this was a small, single-center study, which limits result generalizability, and patients with AL and ATTR could not be evaluated separately because of their small numbers. On the other hand, patients were enrolled prospectively and underwent a standardized characterization. Second, neither histologic analysis nor CMR specifically evaluated myocardial edema or microvascular dysfunction, which might both contribute to ECV increase. Third, ECV at CMR was measured only in the septum, in agreement with current recommendations<sup>38</sup> and previous literature on CA,<sup>8</sup> because this measurement is more reliable than in other LV regions, and in the thin-walled right ventricle. A last limitation is the fact that electron microscopy and mass spectrometry were not available when most of these biopsies were analyzed.

In conclusion, this systematic analysis of LV EMBs in CA shows that extracellular spaces are expanded by fibrosis, and not just by amyloid deposits, and that this combination can better explain myocardial tissue characterization at CMR and circulating levels of biomarkers of cardiac damage.

## ARTICLE INFORMATION

Received December 2, 2020; accepted June 14, 2021.

### Affiliations

University Hospital of Pisa, Pisa, Italy (A.P., C.A.); ; Institute of Life Sciences, Scuola Superiore Sant'Anna, Pisa, Italy (A.A., V.M., A.B., G.V., S.M., C.P., C.P., M.E.); Fondazione Toscana Gabriele Monasterio, Pisa, Italy (A.A., V.M., A.B., G.V., D.G., A.G., C.P., L.E.P., M.A.C., M.C., N.M., C.P., C.P., M.E.); Centro Cardiologico Universitario di Ferrara, University of Ferrara, Italy (C.R.); and Maria Cecilia Hospital, GVM Care & Research, Cotignola, Italy (C.R.).

## Sources of Funding

None.

## Disclosures

None.

## Supplementary Material

Tables S1–S3

Figures S1–S6

## REFERENCES

- Benson MD, Buxbaum JN, Eisenberg DS, Merlini G, Saraiva MJM, Sekijima Y, Sipe JD, Westermark P. Amyloid nomenclature 2018: recommendations by the International Society of Amyloidosis (ISA) nomenclature committee. *Amyloid*. 2018;25:215–219. doi: 10.1080/13506129.2018.1549825
- Maleszewski JJ. Cardiac amyloidosis: pathology, nomenclature, and typing. *Cardiovasc Pathol*. 2015;24:343–350. doi: 10.1016/j.carpath.2015.07.008
- Hahn VS, Yanek LR, Vaishnav J, Ying W, Vaidya D, Lee YZJ, Riley SJ, Subramanya V, Brown EE, Hopkins CD, et al. Endomyocardial biopsy characterization of heart failure with preserved ejection fraction and prevalence of cardiac amyloidosis. *JACC Heart Fail*. 2020;8:712–724. doi: 10.1016/j.jchf.2020.04.007
- Cohen OC, Sharpley F, Gilbertson JA, Wechalekar AD, Sachchithanantham S, Mahmood S, Whelan CJ, Martinez-Naharro A, Fontana M, Lachmann HJ, et al. The value of screening biopsies in light-chain (AL) and transthyretin (ATTR) amyloidosis. *Eur J Haematol*. 2020;105:352–356. doi: 10.1111/ejh.13458
- Yilmaz A, Kindermann I, Kindermann M, Mahfoud F, Ukena C, Athanasiadis A, Hill S, Mahrholdt H, Voehringer M, Schieber M, et al. Comparative evaluation of left and right ventricular endomyocardial biopsy: differences in complication rate and diagnostic performance. *Circulation*. 2010;122:900–909. doi: 10.1161/CIRCULATIONAHA.109.924167
- Rubiś P, Rudnicka-Sosin L, Jurczyszyn A, Janion M, Podolec P. The paramount importance of repeated left ventricular endomyocardial biopsy during the diagnosis of restrictive cardiomyopathy due to AL cardiac amyloidosis. *Kardiol Pol*. 2016;74:796. doi: 10.5603/KP.2016.0114
- Francis R, Lewis C. Myocardial biopsy: techniques and indications. *Heart*. 2018;104:950–958. doi: 10.1136/heartjnl-2017-311382
- Leone O, Veinot JP, Angelini A, Baandrup UT, Basso C, Berry G, Bruneval P, Burke M, Butany J, Calabrese F, et al. 2011 consensus statement on endomyocardial biopsy from the Association for European Cardiovascular Pathology and the Society for Cardiovascular Pathology. *Cardiovasc Pathol*. 2012;21:245–274. doi: 10.1016/j.carpath.2011.10.001
- Lang RM, Badano LP, Mor-Avi V, Afilalo J, Armstrong A, Ernande L, Flachskampf FA, Foster E, Goldstein SA, Kuznetsova T, et al. Recommendations for cardiac chamber quantification by echocardiography in adults: an update from the American Society of Echocardiography and the European Association of Cardiovascular Imaging. *J Am Soc Echocardiogr*. 2015;28:1–39.e14. doi: 10.1016/j.echo.2014.10.003
- Aquaro GD, Camastra G, Monti L, Lombardi M, Pepe A, Castelletti S, Maestrini V, Todiere G, Masci P, di Giovine G, et al. Reference values of cardiac volumes, dimensions, and new functional parameters by MR: a multicenter, multivendor study. *J Magn Reson Imaging*. 2017;45:1055–1067. doi: 10.1002/jmri.25450
- Aquaro GD, Pugliese NR, Perfetto F, Cappelli F, Barison A, Masci PG, Passino C, Emdin M. Myocardial signal intensity decay after gadolinium injection: a fast and effective method for the diagnosis of cardiac amyloidosis. *Int J Cardiovasc Imaging*. 2014;30:1105–1115. doi: 10.1007/s10554-014-0436-6
- Kellman P, Wilson JR, Xue H, Ugander M, Arai AE. Extracellular volume fraction mapping in the myocardium, part 1: evaluation of an automated method. *J Cardiovasc Magn Reson*. 2012;14:63. doi: 10.1186/1532-429X-14-63
- Treibel TA, Kozor R, Schofield R, Benedetti G, Fontana M, Bhuvana AN, Sheikh A, López B, González A, Manisty C, et al. Reverse myocardial remodeling following valve replacement in patients with aortic stenosis. *J Am Coll Cardiol*. 2018;71:860–871. doi: 10.1016/j.jacc.2017.12.035
- Prontera C, Zucchelli GC, Vittorini S, Storti S, Emdin M, Clerico A. Comparison between analytical performances of polyclonal and monoclonal electrochemiluminescence immunoassays for NT-proBNP. *Clin Chim Acta*. 2009;400:70–73. doi: 10.1016/j.cca.2008.10.011
- Giannitsis E, Kurz K, Hallermayer K, Jarausch J, Jaffe AS, Katus HA. Analytical validation of a high-sensitivity cardiac troponin T assay. *Clin Chem*. 2010;56:254–261. doi: 10.1373/clinchem.2009.132654
- Mueller T, Dieplinger B. The Presage® ST2 Assay: analytical considerations and clinical applications for a high-sensitivity assay for measurement of soluble ST2. *Expert Rev Mol Diagn*. 2013;13:13–30.
- Aimo A, Januzzi JL Jr, Bayes-Genis A, Vergaro G, Sciarrone P, Passino C, Emdin M. Clinical and prognostic significance of sST2 in heart failure: JACC review topic of the week. *J Am Coll Cardiol*. 2019;74:2193–2203. doi: 10.1016/j.jacc.2019.08.1039
- Kunnath-Velayudhan S, Larsen BT, Coley SM, De Michele S, Santoriello D, Colby TV, Bhagat G, Saqi A. Masson trichrome and sulfated alcian blue stains distinguish light chain deposition disease from amyloidosis in the lung. *Am J Surg Pathol*. 2021;45:405–413. doi: 10.1097/PAS.0000000000001593
- Misumi Y, Ando Y, Gonçalves NP, Saraiva MJ. Fibroblasts endocytose and degrade transthyretin aggregates in transthyretin-related amyloidosis. *Lab Invest*. 2013;93:911–920. doi: 10.1038/labinvest.2013.83
- Tanaka K, Essick EE, Doros G, Tanriverdi K, Connors LH, Seldin DC, Sam F. Circulating matrix metalloproteinases and tissue inhibitors of metalloproteinases in cardiac amyloidosis. *J Am Heart Assoc*. 2013;2:e005868. doi: 10.1161/JAHA.112.005868
- Li R, Yang ZG, Wen LY, Liu X, Xu HY, Zhang Q, Guo YK. Regional myocardial microvascular dysfunction in cardiac amyloid light-chain amyloidosis: assessment with 3T cardiovascular magnetic resonance. *J Cardiovasc Magn Reson*. 2016;18:16. doi: 10.1186/s12968-016-0240-7
- Austin BA, Duffy B, Tan C, Rodriguez ER, Starling RC, Desai MY. Comparison of functional status, electrocardiographic, and echocardiographic parameters to mortality in endomyocardial-biopsy proven cardiac amyloidosis. *Am J Cardiol*. 2009;103:1429–1433. doi: 10.1016/j.amjcard.2009.01.361
- Cheng Z, Kang L, Tian Z, Chen W, Guo W, Xu J, Chen T, Fang L, Zeng Y, Cheng K, et al. Utility of combined indexes of electrocardiography and echocardiography in the diagnosis of biopsy proven primary cardiac amyloidosis. *Ann Noninvasive Electrocardiol*. 2011;16:25–29. doi: 10.1111/j.1542-474X.2010.00403.x
- Khan T, Selvakumar D, Trivedi S, Rao K, Harapoz M, Thiagalingam A, Denniss AR, Varikatt W. The value of endomyocardial biopsy in diagnosis and guiding therapy. *Pathology*. 2017;49:750–756. doi: 10.1016/j.pathol.2017.08.004
- Schelbert EB, Bering P. Constancy of spatial variation in diffuse myocardial disease: implications for diagnosing disease. *Circ Cardiovasc Imaging*. 2018;11:e007836. doi: 10.1161/CIRCIMAGING.118.007836
- Schwarz F, Mall G, Zebe H, Blicke J, Derks H, Manthey J, Kübler W. Quantitative morphologic findings of the myocardium in idiopathic dilated cardiomyopathy. *Am J Cardiol*. 1983;51:501–506. doi: 10.1016/S0002-9149(83)80088-5
- Duca F, Kammerlander AA, Panzenböck A, Binder C, Aschauer S, Loewe C, Agis H, Kain R, Hengstenberg C, Bonderman D, et al. Cardiac magnetic resonance T<sub>1</sub> mapping in cardiac amyloidosis. *JACC Cardiovasc Imaging*. 2018;11:1924–1926. doi: 10.1016/j.jcmg.2018.06.010
- Martinez-Naharro A, Treibel TA, Abdel-Gadir A, Bulluck H, Zumbo G, Knight DS, Kotecha T, Francis R, Hutt DF, Rezk T, et al. Magnetic resonance in transthyretin cardiac amyloidosis. *J Am Coll Cardiol*. 2017;70:466–477. doi: 10.1016/j.jacc.2017.05.053
- Robbers LF, Baars EN, Brouwer WP, Beek AM, Hofman MB, Niessen HW, van Rossum AC, Marcu CB. T1 mapping shows increased extracellular matrix size in the myocardium due to amyloid depositions. *Circ Cardiovasc Imaging*. 2012;5:423–426. doi: 10.1161/CIRCIMAGING.112.973438
- Fontana M, Banyersad SM, Treibel TA, Maestrini V, Sado DM, White SK, Pica M, Castelletti S, Piechnik SK, Robson MD, et al. Native T1 mapping in transthyretin amyloidosis. *JACC Cardiovasc Imaging*. 2014;7:157–165. doi: 10.1016/j.jcmg.2013.10.008
- Banyersad SM, Fontana M, Maestrini V, Sado DM, Captur G, Petrie A, Piechnik SK, Whelan CJ, Herrey AS, Gillmore JD, et al. T1 mapping and survival in systemic light-chain amyloidosis. *Eur Heart J*. 2015;36:244–251. doi: 10.1093/eurheartj/ehu444
- Hosch W, Hosch W, Kristen AV, Hosch W, Kristen AV, Libicher M, Dengler TJ, Aulmann S, Heye T, Schnabel PA, et al. Late enhancement in cardiac amyloidosis: correlation of MRI enhancement

- pattern with histopathological findings. *Amyloid*. 2008;15:196–204. doi: 10.1080/13506120802193233
33. Hashimura H, Ishibashi-Ueda H, Yonemoto Y, Ohta-Ogo K, Matsuyama TA, Ikeda Y, Morita Y, Yamada N, Yasui H, Naito H, et al. Late gadolinium enhancement in cardiac amyloidosis: attributable both to interstitial amyloid deposition and subendocardial fibrosis caused by ischemia. *Heart Vessels*. 2016;31:990–995. doi: 10.1007/s00380-015-0658-0
  34. Qian G, Wu C, Zhang Y, Chen YD, Dong W, Ren YH. Prognostic value of high-sensitivity cardiac troponin T in patients with endomyocardial-biopsy proven cardiac amyloidosis. *J Geriatr Cardiol*. 2014;11:136–140. doi: 10.3969/j.issn.1671-5411.2014.02.011
  35. Siegismund CS, Escher F, Lassner D, Kühl U, Gross U, Fruhwald F, Wenzel P, Münzel T, Frey N, Linke RP, et al. Intramyocardial inflammation predicts adverse outcome in patients with cardiac AL amyloidosis. *Eur J Heart Fail*. 2018;20:751–757. doi: 10.1002/ejhf.1039
  36. Satoskar AA, Efebera Y, Hasan A, Brodsky S, Nadasdy G, Dogan A, Nadasdy T. Strong transthyretin immunostaining: potential pitfall in cardiac amyloid typing. *Am J Surg Pathol*. 2011;35:1685–1690. doi: 10.1097/PAS.0b013e3182263d74
  37. Dunphy CH. Applications of flow cytometry and immunohistochemistry to diagnostic hematopathology. *Arch Pathol Lab Med*. 2004;128:1004–1022. doi: 10.5858/2004-128-1004-AOFCAI
  38. Messroghli DR, Moon JC, Ferreira VM, Grosse-Wortmann L, He T, Kellman P, Mascherbauer J, Nezafat R, Salerno M, Schelbert EB, et al. Clinical recommendations for cardiovascular magnetic resonance mapping of T1, T2, T2\* and extracellular volume: a consensus statement by the Society for Cardiovascular Magnetic Resonance (SCMR) endorsed by the European Association for Cardiovascular Imaging (EACVI). *J Cardiovasc Magn Reson*. 2017;19:75. doi: 10.1186/s12968-017-0389-8

# Supplemental Material

**Table S1. Comparison between patients undergoing or not undergoing cardiac magnetic resonance (CMR).**

	<b>All patients n=37</b>	<b>CMR n=29 (78)</b>	<b>No CMR n=8 (22)</b>	<b>p</b>
Men, n (%)	34 (92)	27 (93)	7 (88)	0.607
Age (years)	72 (68-81)	71 (64-82)	74 (67-84)	0.704
AL/ATTR, n (%)		16/13 (55/45)	3/5 (38/63)	0.376
eGFR (mL/min/1.73 m <sup>2</sup> )	67 (45-79)	62 (44-84)	49 (41-77)	0.373
NYHA class I-II/III-IV, n (%)		12/17 (41/59)	3/5 (38/62)	0.843
NT-proBNP (ng/L)	6,772 (2,071-12,557)	7,901 (1,294-12,872)	10,055 (5,265-14,800)	0.421
hs-TnT (ng/L)	62 (38-140)	60 (38-173)	79 (34-202)	0.925
sST2 (ng/mL)	27 (16-37)	28 (17-41)	22 (15-33)	0.415
<b>TTE</b>				
E/e'	17 (12-24)	19 (12-24)	17 (13-26)	0.842
LAVi (mL/m <sup>2</sup> )	24 (21-28)	21 (20-26)	28 (24-30)	<b>0.023</b>
Moderate/severe aortic stenosis, n (%)	2 (5)	2 (7)	0 (0)	0.445
TAPSE	17 (13-22)	18 (14-22)	13 (11-18)	0.208

Diphosphonate scintigraphy				
Perugini score 0/1/2/3, n (%)	18/0/5/14 (49/0/14/38)	15/0/3/11 (52/0/10/38)	3/0/2/3 (38/0/25/38)	0.533
Heart-to-controlateral lung ratio	1.36 (1.06-1.91)	1.30 (1.04-1.83)	1.41 (1.09-2.18)	0.604
Extent of amyloid deposits (%)	15 (10-30)	18 (8-30)	23 (8-45)	0.625
Amyloid pattern				
Minimal, n (%)	3 (8)	3 (10)	0 (0)	0.213
Focal, n (%)	1 (3)	0 (0)	1 (13)	
Multifocal, n (%)	29 (78)	23 (79)	6 (75)	
Diffuse, n (%)	4 (11)	3 (10)	1 (13)	
Amyloid location				
Interstitial, n (%)	11 (30)	10 (35)	1 (13)	0.234
Interstitial and perivascular, n (%)	23 (62)	16 (55)	7 (88)	
Interstitial, perivascular, vascular, n (%)	3 (8)	3 (10)	0 (0)	
H score	9 (8-10)	9 (8-10)	10 (8-10)	0.378
Extent of fibrosis (%)	15 (10-23)	13 (10-28)	16 (6-23)	0.704
Extent of amyloidosis and fibrosis (%)	40 (30-49)	40 (23-49)	38 (32-53)	0.957
CD3+ (cells/mm <sup>3</sup> )	6 (5-10)	6 (5-10)	8 (3-13)	0.926

CD68+ (cells/mm <sup>3</sup> )	11 (7-16)	12 (8-15)	10 (7-18)	0.564
--------------------------------	-----------	-----------	-----------	-------

AL, amyloid light chain amyloidosis; ATTR, amyloid transthyretin amyloidosis; ECV, extracellular volume; eGFR, estimated glomerular filtration rate; hs-TnT, high-sensitivity troponin T; IVS, interventricular septum; LGE, late gadolinium enhancement; LVEDVi, left ventricular end-diastolic volume index; LVEF, left ventricular ejection fraction; LVESVi, left ventricular end-systolic volume index; LVMI, left ventricular mass index; NT-proBNP, N-terminal fragment of pro-B-type natriuretic peptide; NYHA, New York Heart Association; PW, posterior wall thickness; RVEDVi, right ventricular end-diastolic volume index; RVEF, right ventricular ejection fraction; sST2, soluble suppression of tumorigenesis-2; SVi, stroke volume index; TAPSE, tricuspid annular plane systolic excursion; TTE, transthoracic echocardiography. (\*) Myocardial T1, ECV, matrix volume and cell volume were available only in 20 subjects.



**Table S2. Histological findings on left ventricle endomyocardial biopsies.**

<b>Patient n</b>	<b>Patient (M/W, age)</b>	<b>AL/ATTR</b>	<b>Amyloid (%)</b>	<b>Fibrosis (%)</b>	<b>Amyloid pattern</b>	<b>Amyloid location</b>	<b>CD3+ (cells/mm<sup>2</sup>)</b>	<b>CD68+ (cells/mm<sup>2</sup>)</b>	<b>H score</b>
1	M, 67	ATTR	15	17	MF	I	5	12	8
2	M, 70	ATTR	10	30	MF	I+PV	8	13	9
3	M, 73	ATTR	10	10	MF	I	7	7	7
4	M, 75	AL	35	10	D	I+PV	39	21	12
5	M, 77	AL	30	5	MF	I+PV	9	7	10
6	M, 85	AL	20	30	MF	I+PV	10	15	12
7	M, 83	ATTR	50	20	MF	I+PV	5	6	9
8	M, 82	ATTR	10	12	MF	I+PV	25	8	9
9	M, 84	ATTR	5	40	MF	I	6	9	8
10	M, 75	ATTR	15	30	MF	I+PV	7	9	9
11	M, 69	AL	30	10	MF	I+PV+V	7	19	9
12	W, 77	ATTR	60	15	MF	I+PV	4	8	9
13	M, 72	AL	15	30	MF	I+PV+V	6	15	8
14	M, 60	AL	10	60	MF	I	41	38	12
15	M, 63	ATTR	5	30	M	I	6	11	7
16	M, 73	AL	30	10	MF	I	9	12	11
17	M, 67	AL	10	10	MF	I+V	3	15	8
18	M, 84	ATTR	10	20	MF	I+PV	9	12	9

19	W, 67	AL	30	5	MF	I	8	18	9
20	M, 83	AL	7	13	MF	I	6	8	7
21	M, 75	ATTR	50	5	D	I+PV	1	4	7
22	M, 51	ATTR	30	20	MF	I	7	13	10
23	M, 67	AL	30	18	MF	I+PV	8	7	10
24	M, 84	ATTR	50	15	MF	I+PV	2	7	8
25	M, 70	AL	35	7	MF	I	3	6	8
26	M, 64	AL	30	15	MF	I+PV	7	13	11
27	M, 80	ATTR	5	9	MF	M	5	10	6
28	W, 72	AL	7	10	F	I+PV	14	34	10
29	M, 69	AL	10	30	MF	I+PV	4	8	8
30	M, 75	ATTR	30	20	MF	I+PV	5	7	10
31	M, 83	ATTR	7	25	MF	I+PV	17	19	11
32	M, 70	AL	10	20	MF	I+PV	5	9	8
33	M, 77	AL	30	10	D	I+PV	10	5	8
34	M, 70	ATTR	40	10	D	I+PV	2	14	9
35	M, 67	AL	7	14	MF	I+PV+V	12	11	8
36	M, 74	AL	5	10	M	I	18	16	9
37	M, 86	ATTR	25	12	MF	I+V	5	9	8

AL, amyloid light-chain; ATTR, amyloid transthyretin; M, man; W, woman. Amyloid pattern: D, diffuse; F, focal; M, minimal; MF, multifocal.

Amyloid location: I, interstitial; PV, perivascular; V, vascular.

**Table S3. Predictors of circulating biomarkers.**

	hs-TnT			NT-proBNP			sST2		
	All	AL	ATTR	All	AL	ATTR	All	AL	ATTR
<b>LGE score</b>	<b>0.006</b>	<b>0.044</b>	0.373	<b>&lt;0.001</b>	<b>0.005</b>	0.451	0.146	0.052	0.772
<b>ECV</b>	<b>0.004</b>	0.089	0.258	<b>0.009</b>	0.200	0.057	0.488	0.808	0.918
<b>Amyloid %</b>	<b>0.005</b>	<b>0.047</b>	0.736	<b>0.044</b>	0.091	0.471	0.093	0.142	0.982
<b>Fibrosis %</b>	0.199	0.267	0.771	0.975	0.985	0.103	0.135	0.453	0.560
<b>Amyloid+fibrosis %</b>	<b>0.035</b>	0.217	0.635	<b>0.002</b>	<b>0.014</b>	0.482	0.265	0.141	0.709
<b>H score</b>	0.337	0.731	0.777	0.054	0.524	0.569	0.954	0.758	0.913
<b>CD3+</b>	0.122	0.266	0.102	0.948	0.840	0.981	0.273	0.847	0.640
<b>CD68+</b>	0.719	0.638	0.477	0.215	0.755	0.712	0.707	0.770	0.273

p values from multivariable linear regression analyses are reported. The model includes left ventricular mass index and ejection fraction. All variables were ln-transformed. AL, amyloid light chain amyloidosis; ATTR, amyloid transthyretin amyloidosis; ECV, extracellular volume; hs-TnT, high-sensitivity troponin T; LGE, late gadolinium enhancement; NT-proBNP, N-terminal fraction of pro-B-type natriuretic peptide; sST2, soluble suppression of tumorigenesis-2.

**Figure S1. Examples of pre-contrast (native) and post-contrast T1 maps and extracellular volume maps.**

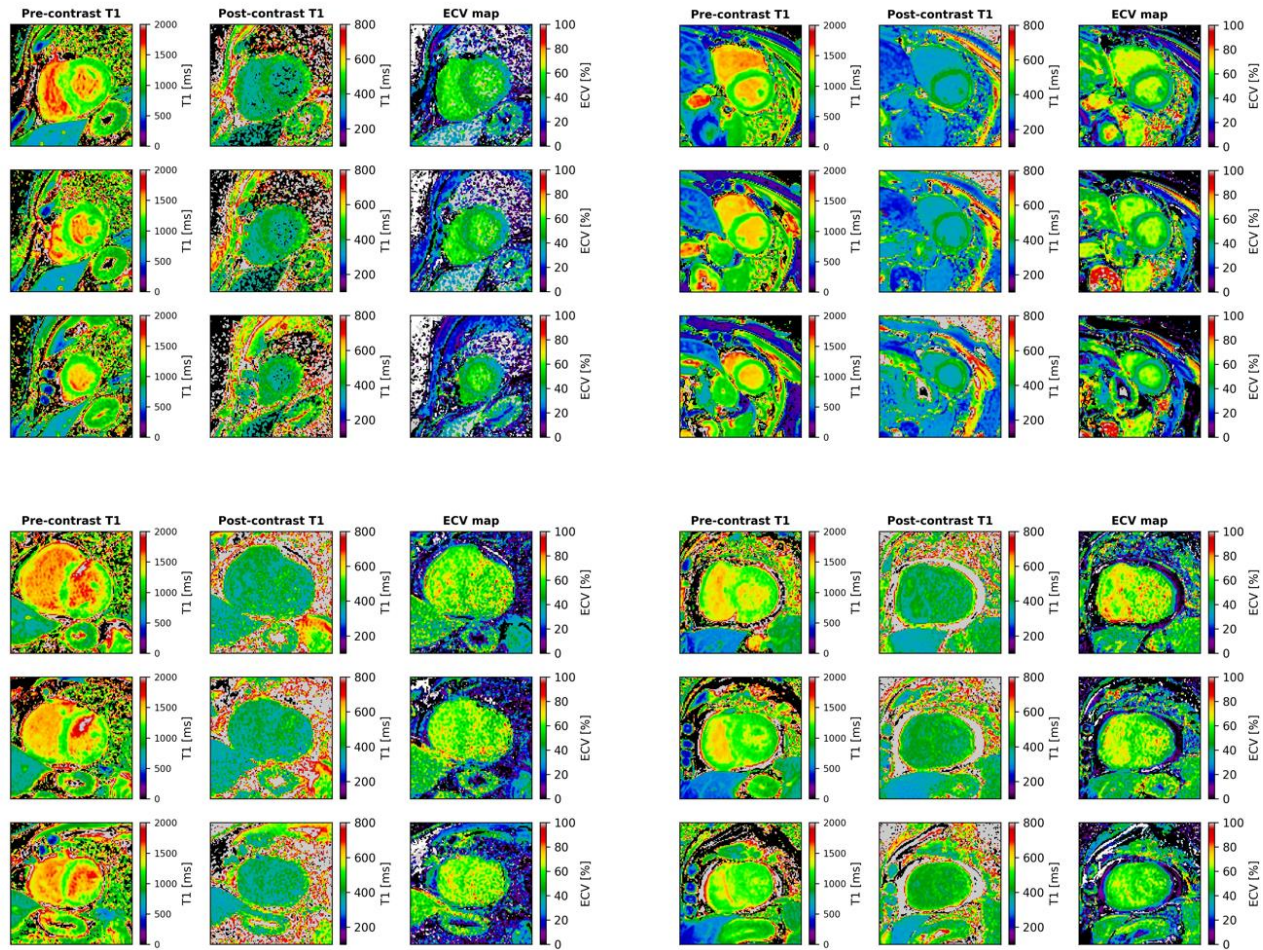


**Figure S2. Endomyocardial biopsy showing diffuse immunoreactivity for lambda Ig light-chains (A) and negative immunostaining for kappa Ig light-chains (B) (Immunoperoxidase staining with hematoxylin counterstaining, original magnification 20x).**

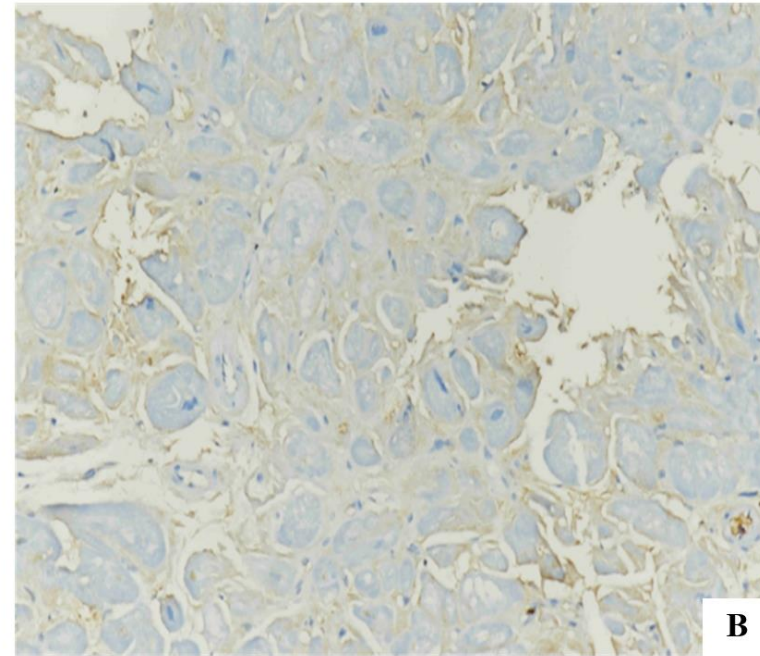
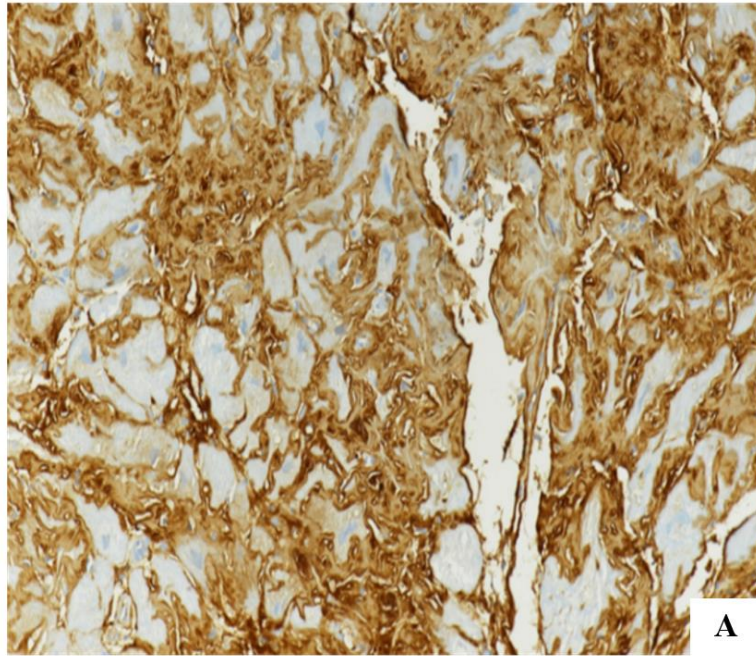
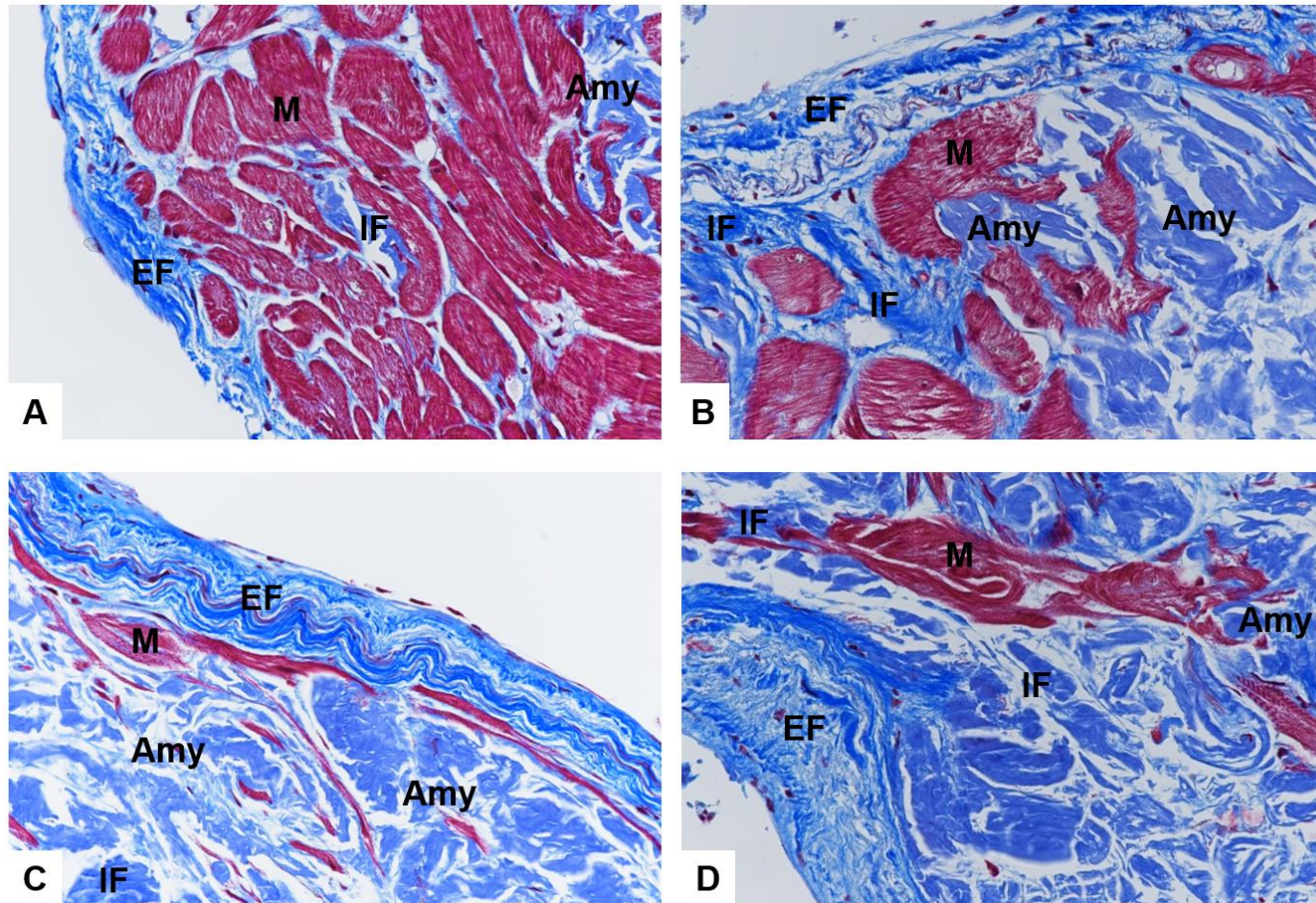


**Figure S3. Focal (A) and mild (A-D) endocardial fibrosis (EF), associated with amyloid deposits (Amy) and interstitial fibrosis (IF) in a left ventricular endomyocardial biopsy.**



Masson's trichrome staining, original magnification 40x.

**Figure S4. Plurifocal interstitial CD3+ lymphocytes in lambda+ CA (A) versus very few and scattered CD3+ lymphocytes in a TTR+ CA (B)**  
(Immunoperoxidase staining with hematoxylin counterstaining, original magnification 40x).

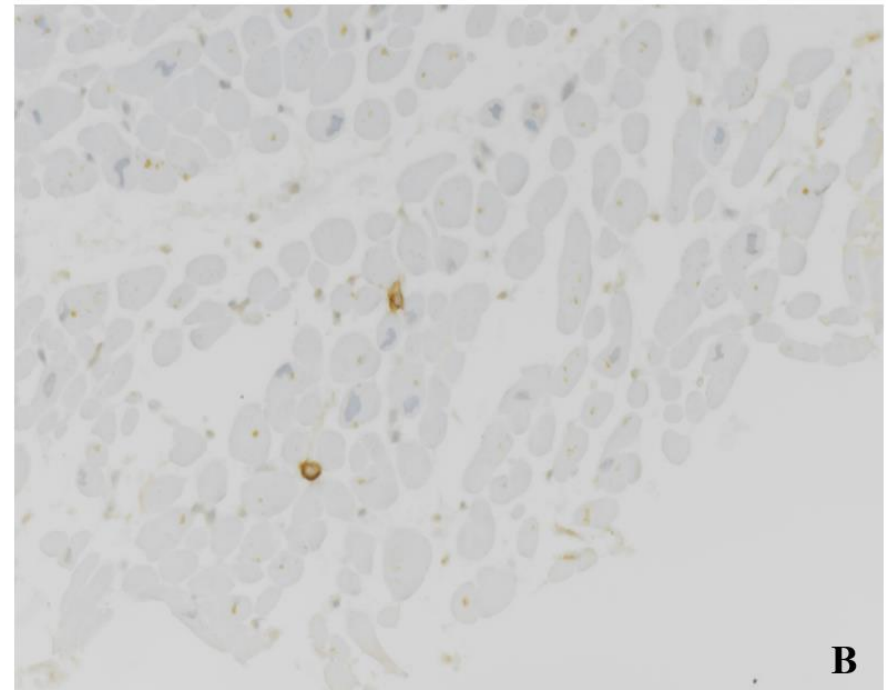
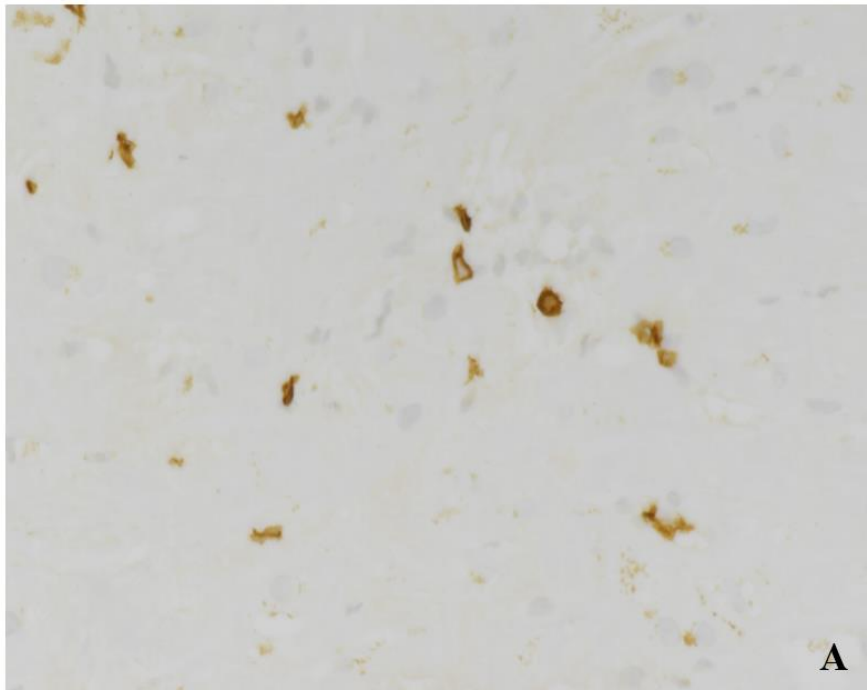
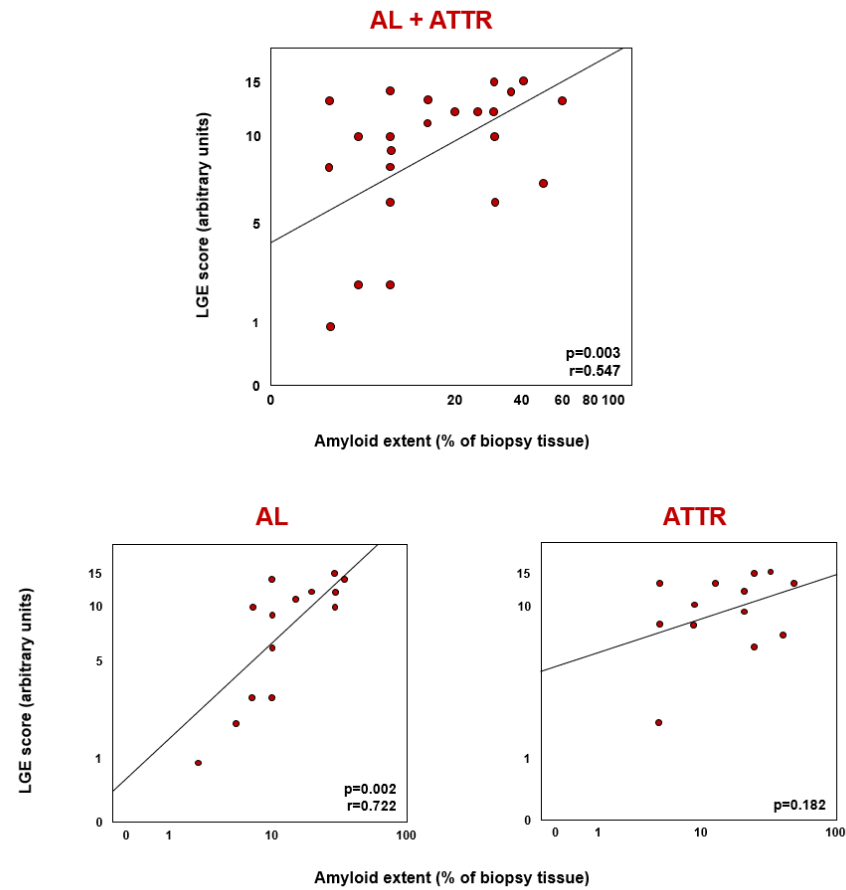


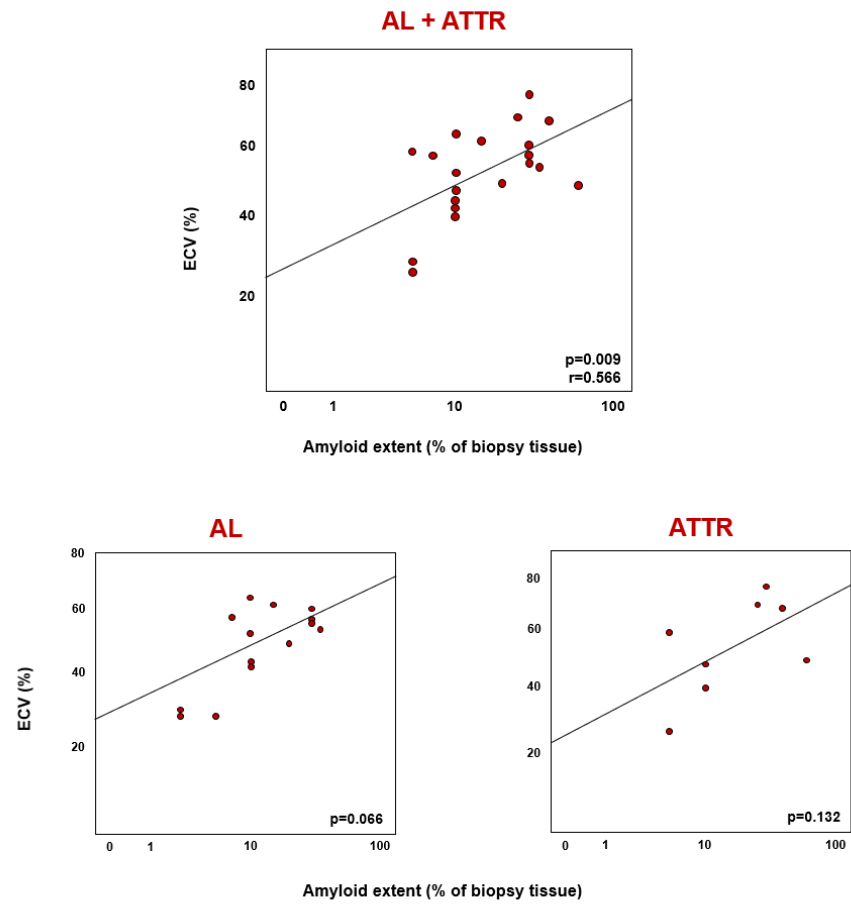
Figure S5. Correlations between the extent of amyloid deposits and late gadolinium enhancement (LGE) score.



AL, amyloid light chain amyloidosis; ATTR, amyloid transthyretin amyloidosis.



**Figure S6. Correlations between the extent of amyloid deposits and extracellular volume (ECV).**



AL, amyloid light chain amyloidosis; ATTR, amyloid transthyretin amyloidosis.